

NUMERICAL SIMULATION OF INTACT ROCK BEHAVIOUR VIA THE CONTINUUM AND VORONOI TESSELLATION MODELS: A SENSITIVITY ANALYSIS

Teja Fabjan (corresponding author)

Formerly at IRGO Consulting, d.o.o.
Slovenčeva 93, 1000 Ljubljana, Slovenia
E-mail: tejafabjan@gmail.com

Diego Mas Ivars

Itasca Consultants AB
Isafjordsgatan 39B, SE-164 40 Kista, Sweden
E-mail: diego@itasca.se

Vladimir Vukadin

Institute for Mining, Geotechnology and Environment
Slovenčeva 93, 1000 Ljubljana, Slovenia
E-mail: vlado.vukadin@irgo.si

Keywords

distinct-element method, parametric sensitivity analysis, intact rock, Voronoi tessellation, micromechanical properties, standard laboratory test

Abstract

The numerical simulation of intact rock microstructure and its influence on macro-scale behaviour has received a lot of attention in the research community in recent years. Generating a grain-like structure with polygonal area contacts is one of the avenues explored for describing the rock's microstructure. A Voronoi tessellation implemented in the Universal Distinct-Element Code (UDEEC) is used to generate models with a polygonal microstructure that represent intact rock. The mechanical behaviour of the Voronoi polygons is defined by micro-properties, which cannot be measured directly in the laboratory. A numerical calibration procedure is needed to produce the macroscopic response of a model that corresponds to the material behaviour measured during a laboratory experiment. In this research, Brazilian, direct tensile, uniaxial compressive and biaxial test models are constructed to simulate the intact rock behaviour under a standard laboratory stress. An extensive series of parametric sensitivity analyses are executed in order to understand the influence of the input micro-properties on every model test behaviour and predict the relation between the micro-properties and the model's macro response. The results can be treated as general guidelines for a complete and efficient intact rock calibration procedure. In parallel, a continuum-based model using the Mohr-Coulomb constitutive relationship is running as a benchmark. It has been shown that the Voronoi-based models through their microstructure approach better reproduce the Brazilian to direct tensile strength ratio, and show a better representation of the dilation, crack pattern and post-peak behaviour in comparison to continuum models.

1 INTRODUCTION

It is well known that even apparently intact rock is heterogeneous on the scale of the grains [1-3]. Grain shape, grain minerals and different types of other defects included in the matrix introduce a heterogeneity in the internal stress distribution [4]. This has a direct influence on the mechanical behaviour of the intact material in terms of fracture initiation and fracture growth, which control the rock's failure, deformability and crack pattern under loading [5, 6]. All these features control the mechanical behaviour of intact rock.

In the past two decades numerical simulations of intact rock microstructure have received a lot of attention from the research community. Many different models have been developed, ranging from the early models based on the continuum finite-element method, to the more recent distinct- or particle-element method models.

Continuum-based models (e.g., RFPFA, [7]; R-T2D, [8]; DIGS, [4]) can simulate the rock failure process by introducing the heterogeneity of rock properties and using the principles of linear elastic fracture mechanics (LEFMs). The medium is assumed to be composed of many mesoscopic elements with different material properties [9]. Local mechanical parameters, both in terms of elastic and strength properties, are reduced following a stochastic distribution, e.g., a Weibull distribution [3, 9]. However, the choice of input properties can be subjective and highly dependent on the statistical distribution of the parameters [3]; furthermore, the complete detachment of the square-shaped elements is truncated.

Since Potyondy & Cundall [10] showed that rock-like material can be successfully modelled with the Bonded Particle Model (BPM), a significant improvement was achieved in modelling the microstructure of rock material. The BPM uses the distinct-element method, as implemented in PFC [11], where a continuum constitutive model is replaced by a simple particle/contact logic [12, 13]. The BPM assumes that the rock behaves like a cemented granular material, where rigid circular or spherical particles are bonded together at their contact points [10]. Reaching the desired material macro-scale behaviour is achieved through a calibration of the input micro-properties [14, 15, 16].

However, when the material is calibrated to the uniaxial compressive strength, the standard BPM significantly over predicts the tensile strength, gives very low triaxial strengths and the failure envelope is linear [17, 18]. By introducing a clumped-particle geometry, or particle cluster logic, in combination with the BPM, these limitations are significantly reduced [10, 18]. Even with the use of clumped-particles and clusters the BPM still suffers from a limitation to match the low ratio of tensile to compressive strength [6], the lowest reachable being at 1/14 [18]. Ratios reported in the literature have much larger variations, ranging from 1/50 to 1/3, depending on rock type, porosity, grain size and other heterogeneities in the rock microstructure [19, 20].

Significant contributions were made by introducing the Grain-Based Model (GBM), where circular/spherical-shaped particles are grouped into polygons with angular boundaries [6]. In this manner, polygonal grains resemble the mineral structure as observed in crystalline rock [12]. Nevertheless, GBM can still not match the Brazilian strength-to-compressive-strength ratio observed in the laboratory [21]. Recently, the BPM has been further developed by incorporating the flat-joint model for grain contacts, allowing for the introduction of a polygonal grain structure that improves the tensile-to-compressive-strength ratio [22].

On the other hand, polygon-shaped grains can be generated directly by using the Voronoi or Delaunay tessellation generators already implemented in the Universal Distinct-Element Code (UDEC) [23]. Polygonal random-shaped particles are interlocked with area contacts that are defined by well-known geomechanical input properties (e.g., cohesion, tensile strength, friction angle, etc.). Lan et al. [2], Kazerani & Zhao [12, 24], Alzo'ubi [25], Kazerani [13] and Gao [26] reported promising results in terms of reaching a reasonable tensile-to-compressive-strength ratio, curved failure envelope, common failure pattern observed in rocks, etc.

The purpose of our study was to evaluate the potential of the Voronoi tessellation model for the simulation of intact rock behaviour. Therefore, a detailed parametric study of the input parameters and their influence on the model's macro behaviour is carried out. The mechanical behaviour of a generic intact rock is simulated by the distinct-element method using UDEC. The rock material is subjected to four standard laboratory test models: Brazilian, direct tensile, uniaxial compressive and biaxial. In parallel, a continuum-based model using a Mohr-Coulomb constitutive relation is running as a benchmark.

2 NUMERICAL MODELLING

Numerical distinct-element method simulations are performed using the two-dimensional software UDEC [23]. In UDEC, the mechanical behaviour of a discontinuous system is represented by (a) the behaviour of discontinuities (contacts) and (b) the behaviour of solid material (grains, polygonal particles, blocks). The contact behaviour is described by any joint model, while blocks may be assumed as rigid or deformable. If deformable blocks are chosen, consisting of triangular finite-strain elements (zones), a constitutive behaviour should be defined by using any available constitutive continuum model or user-defined model. As with any other discrete element code, it allows finite displacements and rotations of discrete blocks, including complete detachment, and recognizes new contacts automatically as the calculation progresses [23].

2.1 Time-marching algorithm

UDEC follows an explicit time-marching scheme that solves the equation of motion directly and is identical to that used by the explicit finite-difference method for continuum analyses. The movement disturbance of a discontinuous system is caused by the applied loads or

body forces. At the start of each time step the procedure first recognizes the new contact locations from known, fixed, block positions. The force-displacement law is then applied to each contact that generates new contact forces. Based on the resultant force and the moment at the block centroids arising from the known forces acting on them, Newton's second law is applied to all the blocks. The velocity and angular velocity are updated and the linear and angular accelerations are calculated. At this point a calculation step could be repeated by calculating the new block location and the block rotation based on the known velocity and angular velocity. If the blocks are deformable, the motion is calculated at the grid points of triangular elements within the block, and the block material constitutive relations give new stresses within the elements [11, 23].

One time step is needed for every cycle around the loop. The time step is limited by the assumption that velocities and accelerations are constant within the time step. To avoid dynamic effects and to reach quasi-static conditions, each time-step increment should be sufficiently small so that disturbances cannot propagate between one discrete element and its intermediate neighbours. The procedure is repeated until either a satisfactory state of equilibrium or one continuing failure results [23].

2.2 Constitutive behaviour of intact rock

UDEC allows for many possibilities to represent block behaviour by using any of the already-implemented constitutive models. In this study the intact rock is modelled with both continuum and Voronoi tessellation approaches. In the continuum approach the intact block behaviour is assumed to follow the conventional Mohr-Coulomb constitutive model, and is from here on denoted as the continuum model. In summary, the general concept follows a set of linear equations in the principal stress space, $\sigma_1, \sigma_2, \sigma_3$, where the shear failure of the isotropic elastic material is controlled by the cohesion c and the friction angle φ in the shear yield function:

$$f_s = \sigma_1 - \sigma_3 \left(\frac{1 + \sin \varphi}{1 - \sin \varphi} \right) + 2c \sqrt{\frac{1 + \sin \varphi}{1 - \sin \varphi}} \quad (1)$$

Tensile failure is controlled by the tension yield function, where the minor principal stress σ_3 cannot exceed the tensile strength σ^t :

$$f_t = \sigma_3 - \sigma^t \quad (2)$$

More details about the Mohr-Coulomb failure criterion can be found in the software manuals [23] or elsewhere (e.g., [27]).

On the other hand, the rock microstructure is modelled as an assemblage of distinct deformable polygons, and is subsequently denoted as the Voronoi model. UDEC has an in-built, automatic generator of the Voronoi tessellation pattern, where a particular region in a model can be subdivided into randomly sized polygons. In such a manner, polygons can represent grains, assemblies of grains and/or other flaws (i.e., defects) in the intact rock that are randomly disturbed over the sample [4, 23] (Fig. 1).

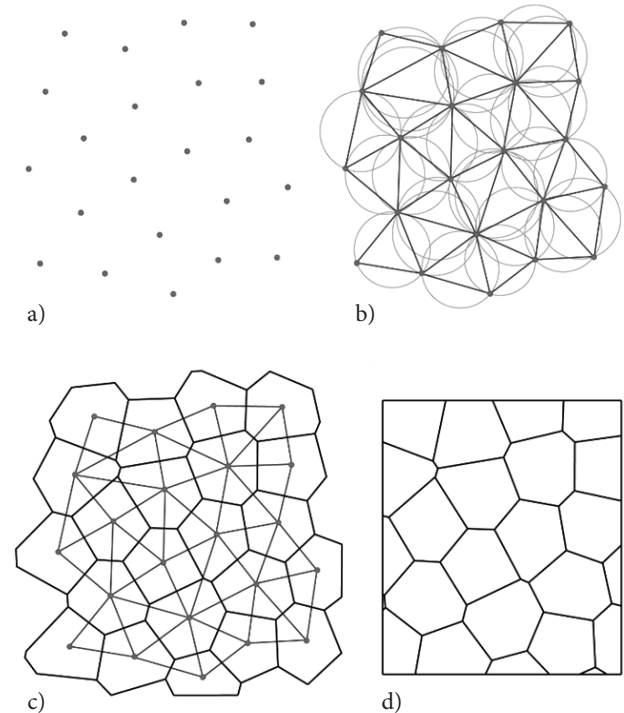


Figure 1. Schematic presentation of Voronoi tessellation generator logic used in UDEC: (a) random generation of points controlled by seed number, (b) generation of Delaunay triangulation, (c) generation of Voronoi tessellation and (d) Voronoi polygons model block [28].

The Voronoi algorithm begins by distributing points within the tessellation region (Fig. 1a). The seed number should be inserted as an input value to set the seed for the random-number generation used by the Voronoi tessellation. During this step the points are allowed to be moved according to the iteration procedure. A larger number of iterations will generate a more uniform spacing between the points and therefore a more uniform tessellation will be generated. These points are then interconnected with lines that form triangles, called Delaunay triangulation, and thus each triangle is circumscribed within a circle containing its three vertices (Fig. 1b). Finally, the Voronoi polygons are created by constructing perpendicular bisections of all the triangles that share a

common side (Fig. 1c). The polygons are truncated at the boundaries of the tessellation region (Fig. 1d) [23].

The Voronoi polygons are assigned an isotropic elastic deformable material model, which means that failure on the micro-scale only takes place at the polygon boundaries, not inside them.

The Voronoi contacts are assumed to behave following the Coulomb slip area joint model. The stress-displacement relation in the normal and shear directions is assumed to be linear and governed by the normal stiffness k_n and the shear stiffness k_s such that:

$$\Delta\sigma_n = -k_n\Delta u_n \quad (3)$$

$$\Delta\tau_s = -k_s\Delta u_s^e \quad (4)$$

where $\Delta\sigma_n$ is the effective normal stress increment, $\Delta\tau_s$ is the effective shear stress increment, Δu_s^e is the elastic component of the incremental shear displacement and Δu_n is the normal displacement increment. However, the normal stress is limited by a limiting tensile strength (if $\sigma_n < -\sigma_t$, then $\sigma_n = 0$) and the shear stress is limited by a linear combination of the cohesion c and the friction angle φ :

$$|\tau_s| \leq c + \sigma_n \tan\varphi = \tau_{\max} \quad (5)$$

When the shear stress exceeds the maximum shear stress ($|\tau_s| \geq \tau_{\max}$) then:

$$\tau_s = \text{sign}(\Delta u_s)\tau_{\max} \quad (6)$$

where Δu_s is the total incremental shear displacement. In addition, joint dilation may occur at the onset of the slip of the joint. The accumulated dilation ψ is limited either by a high normal stress level or a large accumulated shear displacement that exceeds a limiting value u_{\max} . Therefore, if $|\tau_s| \leq \tau_{\max}$ or $|\tau_s| = \tau_{\max}$ and $|u_s| \geq u_{\max}$, then $\psi = 0$, otherwise $\psi > 0$.

3 NUMERICAL LABORATORY

The characterisation of intact rock is achieved by performing standard laboratory tests, so the aim of this study is to recreate the same testing procedure within a numerical environment using the distinct-element method. Therefore, four standard laboratory test models are developed: a splitting tensile strength test (Brazilian test), a direct tensile test, a uniaxial compressive strength (UCS) test and a biaxial test. These tests characterise the rock material in the tensile and compressive stress paths and can be used to calibrate the constitutive behaviour of the modelled material to the real material.

3.1 Model generation

Two types of model geometry are generated. A circle-shaped model is used to simulate the Brazilian test and a rectangular-shaped model is used to simulate the direct tensile test, the UCS test and the biaxial test. Plane stress analyses are adopted for all the cases to assume thin model samples. These models are run by applying a vertical velocity at the external boundary at the top of the sample. The velocity is fixed and set to zero in the vertical direction at the external boundary at the bottom of the sample. The only difference between the tests is the direction of the applied velocity. The velocity is directed upwards in the direct tensile test to produce tensile conditions in the sample, while in the other test models the velocity is directed downwards to generate a compressive stress state. In addition, to ensure confinement in the biaxial test model, a horizontal compressive stress is acting on the left and right external boundaries, and the vertical horizontal compressive stress acts on the top external boundary of the model sample. The boundary conditions are shown in Fig. 2.

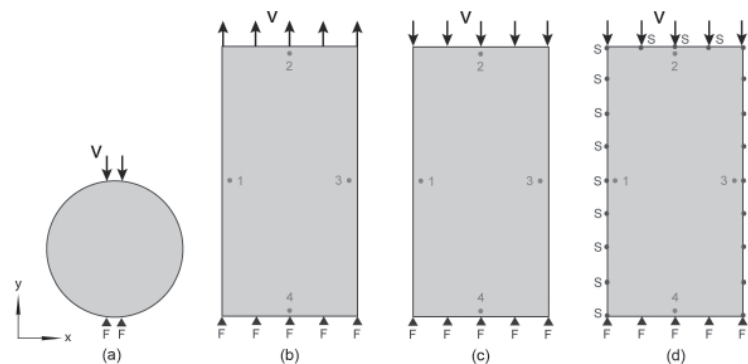


Figure 2. Boundary conditions in (a) Brazilian test, (b) direct tensile test, (c) uniaxial compressive test and (d) biaxial test. "F" denotes fixed grid points and "S" denotes confinement stress boundary conditions. Numbers on samples show locations of monitoring grid points.

3.2 Monitoring

The monitoring procedure is very similar in all the test models, where the grid-point forces, the displacement and the positions of the grid points are monitored using a FISH function. Based on these monitored data points the strength and deformation properties are calculated for every time step while running the test analysis.

The applied vertical velocity at the top of the sample causes a reaction force at every grid point in the sample. In each time step the total sum of the vertical forces F_y for every grid point at the external boundary on the top side of the sample is divided by the cross-section d of the sample to obtain the vertical stress σ_y . The peak stress is determined as the failure strength of the tested material. However, in the Brazilian test model the reaction force is converted into stress by using the standard Brazilian strength σ_B equation [29]:

$$\sigma_B = 2F_y / \pi dt \quad (7)$$

where F_y is the total sum of the vertical forces, d is the sample (circle) diameter and t is the sample thickness, which is assumed to be unity in a 2D analysis.

Material deformability is calculated by monitoring the displacements and the positions at the grid points in the middle of every side of the sample, as shown in Fig. 2. The horizontal deformation is calculated based on monitoring locations 1 and 3, and the vertical deformation is calculated based on monitoring locations 2 and 4. The Young's modulus is then calculated by dividing the axial stress by the vertical deformation, and the Poisson's ratio is calculated by dividing the horizontal deformation by the vertical deformation.

4 NUMERICAL PARAMETRIC SENSITIVITY ANALYSIS

An extensive series of parametric sensitivity analyses are executed in order to understand the influence of the input properties on the model's behaviour and the relationship between the micro-properties and the model's macro response. This kind of study has given us a set of general guidelines for the calibration procedure of the intact material. Parallel to this, a series of analyses on continuum models are carried out to compare the results with those of the Voronoi model.

The parametric sensitivity analysis is conducted by running a series of simulations in which each significant input parameter is varied systematically over a chosen range, while all the other parameters were fixed. Some of the ranges used here are not realistic for rock-like material.

However, as will be shown later, some valuable insights into the numerical environment can be obtained from them. Two types of parameters were tested for all four numerical laboratory tests: (a) numerical input properties (particle size, seed number, number of iterations, mesh density, number of fixed grid points, strain rate, model sample size and shape) and (b) material input properties (material density, Young's modulus, Poisson's ratio, normal and shear stiffness, cohesion, friction angle, tensile strength and dilation). The input properties for both the continuum and the Voronoi models are arbitrarily chosen within a range that can represent the behaviour of sedimentary rock, such as marl, siltstone, etc. The input properties are listed in Table 1 and Table 2 (next page) for the continuum and Voronoi models, respectively.

Table 1. Input properties used in the parametric sensitivity analysis for the continuum model.

Parameter	Input value of parameter	Tested range of parameter
<i>Numerical input properties</i>		
Model height (mm)	500	50–1,500
Model width/diameter (mm)	250	25–750
Zone edge length (mm)	10	10–4,000
Applied velocity (m/s)	0.001 ^a	0.00–0.3
<i>Material input properties</i>		
Material density (kg/m ³)	2,548	10–100,000
Young's modulus (GPa)	8.940	1–100
Poisson's ratio ()	0.167	0.1–0.4
Cohesion (MPa)	2.2	0.5–20
Friction angle (°)	30	0–80
Limit tensile strength (MPa)	1.5	0.1–20
Dilation angle (°)	2	0–15

^a Applied velocity for UCS test and biaxial test was 0.005 m/s.

4.1 Size of the Voronoi polygons

The resolution of the model is controlled by the size of the Voronoi polygons and it affects the peak strength and the material deformability. The size of the Voronoi polygons is defined by the Voronoi edge length, which must be at least 20 times that of the corner rounding length and specifies the input value of the average edge length of the Voronoi polygons [23]. A higher model resolution requires more cycles (time) to reach mechanical equilibrium, and also needs more time to generate the initial polygon packing in a model than a lower model resolution.

Thus, a series of analyses are run to determine the optimal model resolution. A minimum of ten seed distributions within any test model were analysed. As will be explained later, different seed numbers give

Table 2. Input micro-properties used in the parametric sensitivity analysis for the Voronoi model.

Parameter	Input value of parameter	Tested range of parameter
<i>Numerical input properties</i>		
Model height (mm)	500	50–25,000
Model width/diameter (mm)	250	25–12,500
Voronoi edge length	16.5	6.25–80
Zone edge length (mm)	8.25	3–125
No. of iterations ()	80	13–1000
Seed no. ()	222	10–999
Applied velocity (m/s)	0.001 ^b	0.001–0.01
<i>Material input properties</i>		
Material density (kg/m ³)	2,548	10–100,000
Young's modulus of polygons (GPa)	9.2	1–100
Poisson's ratio of polygons ()	0.2	0.1–0.4
Normal stiffness (GPa/m)	10,000	100–100,000
Shear stiffness (GPa/m)	2,000	20–200,000
Contact cohesion (MPa)	2.2	0–10
Contact friction angle (°)	10	0–80
Contact limit tensile strength (MPa)	1.5	0.1–20
Dilation angle (°)	2	0–15

^b Applied velocity for UCS test and biaxial test was 0.005 m/s.

different peak strengths, so the mean peak strength and the relative standard deviation (RSD) are calculated from the results of the tests. In order to give a better representation of the results from all the model tests, the peak strength values are normalized to the mean value.

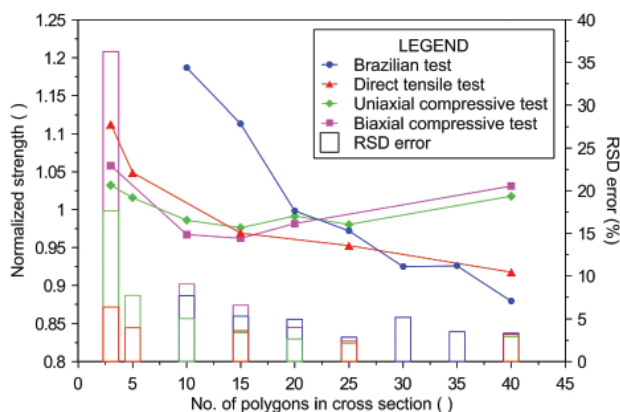


Figure 3. Effect of polygon size resolution on normalized peak strength and corresponding RSD error for the Voronoi model.

The results for all four tests shown in Fig. 3 imply that at least 10 Voronoi polygons along the cross-section of a model are required to minimize the polygon resolution's influence on the peak strength to an acceptable level. In this range the RSD begins to stabilize at around 5 %. However, both the uniaxial compressive and biaxial model tests show a slight increase in the peak strength when the number of Voronoi polygons is larger. That effect is marginal and might be a result of statistical repetition. When more Voronoi elements are included, the fracture (i.e., the failure surface) can have a different path and the resulting peak may be slightly different.

Based on this, the recommended model resolution is between 10 and 25 Voronoi polygons per model sample cross-section. A denser Voronoi size resolution can be used, but it will lead to increased calculation times. According to the ASTM standard [30] and ISRM suggested methods [31], the sample diameter tested in the laboratory should be larger than the largest mineral grain by at least 10 or 20 times. If it is assumed that the Voronoi polygons represent grains, this will be in agreement with the presented results.

However, the results from the Brazilian strength (Fig. 3) do not show the same trend as the other model tests. The strength keeps decreasing, even though a maximum of 40 Voronoi polygons per model test cross-section are tested. The reason for the decreasing trend of the Brazilian strength might be due to the fact that there are fixed grid points at the external boundary, which are located on a curved line due to the circular model geometry. The same response is observed in the Brazilian model tests with the Dalanauy triangles [12]. However, to keep the consistency in the results from every model test in the numerical laboratory, the polygon resolution was kept equal to 15 from this point on in the study for all the samples tested.

The same as in the BPM models [10], the particle size resolution slightly influences the elastic properties. Increasing the polygon resolution up to 40, the Young's modulus decreases and the Poisson's ratio increases, both by approximately 15 % (Fig. 4). A possible explanation for this behaviour might be as follows. While the polygon resolution is increasing, more contacts are formed in the model. Therefore, the model sample has a greater ability to deform due to the displacement along the contacts, which cause a lower Young's modulus and a higher Poisson's ratio.

4.2 Microstructure heterogeneity

The heterogeneity of intact rock at the grain scale is due to the grain shape and size, the grain contact length and orientations, the constituent minerals and other

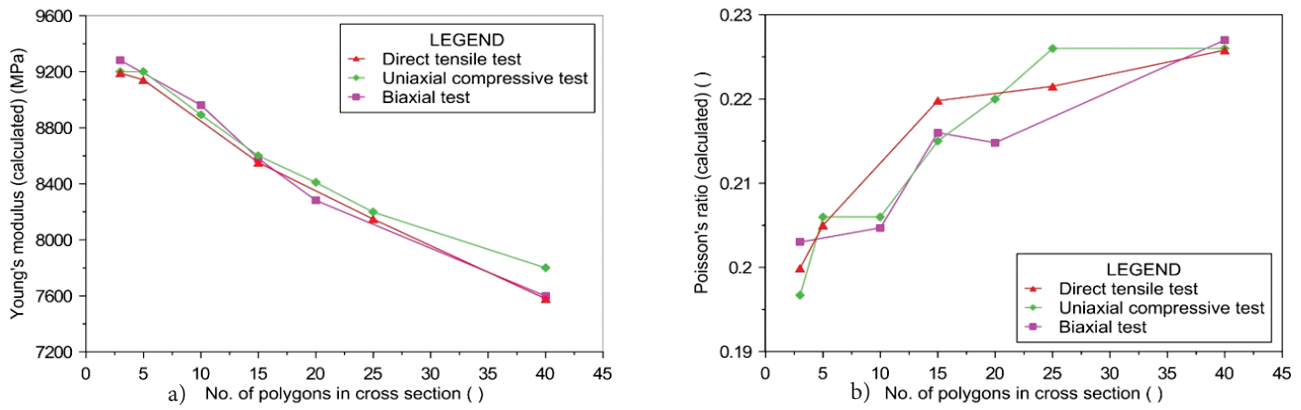


Figure 4. Effect of polygon size resolution on (a) Young's modulus and (b) Poisson's ratio for the Voronoi model.

spatial defects [2]. In the Voronoi model the material's geometric heterogeneity and the polygon distribution can be controlled by the seed number and the number of steps in the iteration procedure applied in the Voronoi tessellation generation.

Every seed number generates a random array of Voronoi tessellation and thus every tested model will give a slightly different macro response, e.g., every seed number will produce a different peak strength, crack pattern, etc., as can be seen from Fig. 5. As previously mentioned, using the recommended polygon resolution (10 to 25) an approximately 5 % RSD error in the peak strength is expected by testing the model with a different seed number. Similarly, the variability of the results due to microstructure heterogeneity occurs in the laboratory as well, because in reality every sample has a slightly different microstructure. Therefore, the distributions of results can be compared to the variations observed in the laboratory tests.

However, the major difference between the numerical and laboratory results is in the size of the variability of the results. In the laboratory the size of the variations is greatly affected by the grain size and other micro-cracks in the rock. This means that some rocks will have a smaller variation than others [28, 32]. On the other hand, as can be seen from Fig 3., the RSD error (which is basically the size of the variations of the results) is going to stabilize when the number of Voronoi polygons is more than 10 polygons per sample cross-section. Therefore, in numerical simulations, following the approach proposed in this paper, we will get approximately the same RSD error, no matter what kind of rock we would like to model.

On the other hand, the number of iterations controls the Voronoi tessellation uniformity, as can be seen from Fig. 6. Increasing the number of iterations reduces the heterogeneity, modifies the crack pattern and influences the peak strength. In general, increasing the iteration

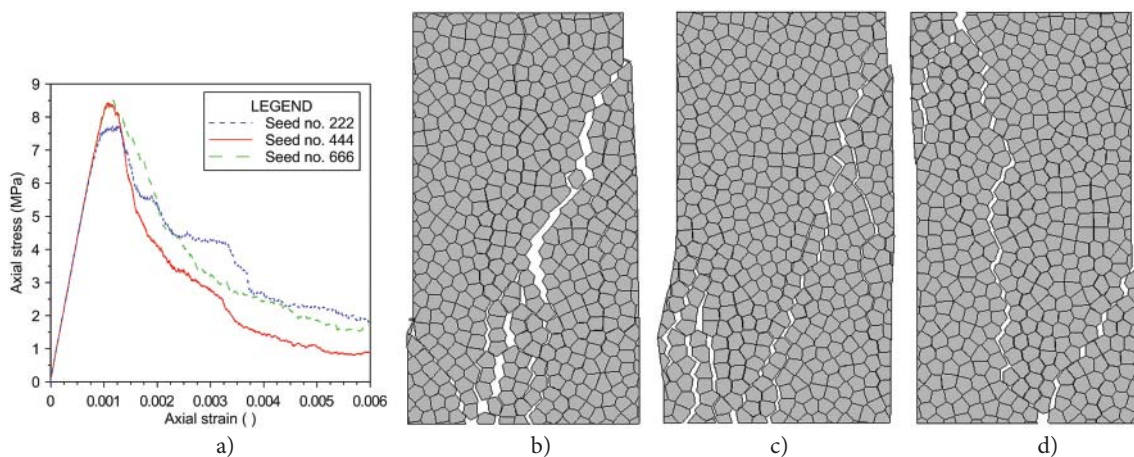


Figure 5. Effect of seed number on (a) uniaxial compressive test stress-strain curve and corresponding model geometry at failure for seed number (b) 222, (c) 444 and (d) 666.

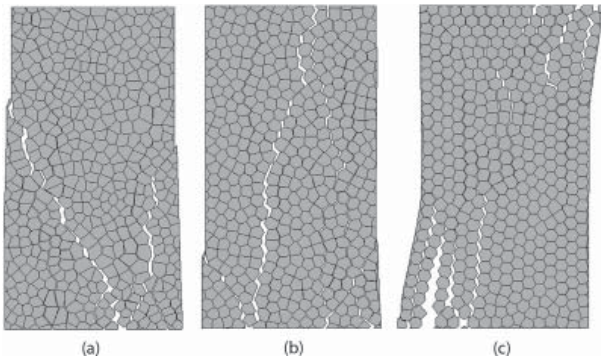


Figure 6. Example of uniaxial compressive test model sample at failure tested with the same seed number, but different iteration number (a) 13, (b) 150 and (c) 800.

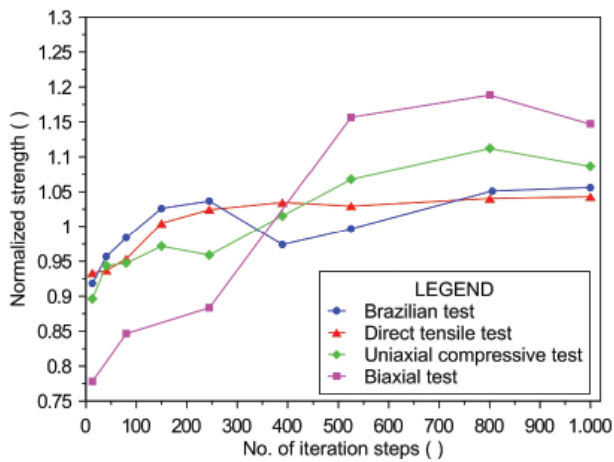


Figure 7. Effect of number of iteration steps on normalized peak strength for the Voronoi model.

number increases the peak strength in all the model tests. The peak strength tends to stabilize using a large number of iteration steps. In tensile tests (e.g., the direct tensile and Brazilian tests) stabilisation is reached after 150 iterations, but in compressive tests (e.g., the UCS and biaxial test) stabilisation is not reached until 550 iteration steps are applied (Fig. 7). This response can be directly linked to the tessellation geometry, where the difference in the geometry becomes more and more insignificant, when comparing two Voronoi tessellations generated with a very high iteration number (higher than 600 iteration steps). Moreover, increasing the number of iteration steps has a negligible influence on the peak-strength scatter between the different seed numbers, and over the entire tested range this is approximately 5 % of RSD.

In most cases, rocks have a heterogeneous microstructure geometry [2]. This can be controlled with the number of iterations. According to this study, less than 250

iterations are recommended to produce natural material behaviour. Iteration numbers between 50 and 250 generate a relatively homogeneous model microstructure, which can be compared to sedimentary rocks (Fig. 6b). A small number of iterations (below 50) generates a more heterogeneous model microstructure, similar to magmatic rocks, e.g., granites (Fig. 6a), but gives a lower peak strength. Finally, a very high iteration number (more than 250) can produce unnatural crack patterns that are normally not observed in real rock (Fig. 6c).

4.3 Mesh density

The blocks/polygons in both the continuum and Voronoi models are discretized into deformable, triangular, finite-difference zones and its zone edge length is one of the input parameters for the model (Fig. 8). To achieve reasonable calculation times and stable numerical results, an optimal zone edge length (mesh density) must be defined for the present model size. For that reason a sensitivity analysis of the zone edge length's influence on all the model tests is carried out.

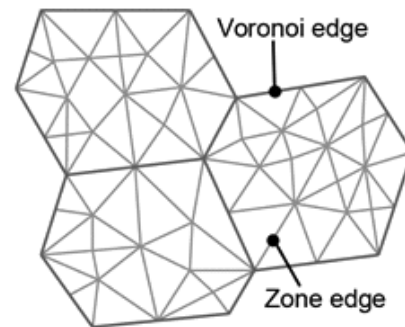


Figure 8. Schematic representation of Voronoi polygon blocks discretized into deformable triangular finite-difference zones.

The sensitivity analysis with the continuum model has shown that the influence of mesh density within the range considered in this study of the peak strength and deformability can be neglected in rectangular-shaped samples (Fig. 9), e.g., direct tensile test, uniaxial compressive test and biaxial test, but it is evident in circular model samples, e.g., the Brazilian test model (Fig. 10). Since the mesh density does not affect the peak strength and deformability in the rectangular model samples within the range considered in this study, the same mesh density can be used, regardless of the model size. However, increasing the model size with a fixed zone edge will affect the peak strength in the Brazilian test model. Therefore, the results for all the test models will be consistent if the appropriate mesh density for the Brazilian test model is found and then used in other test models.

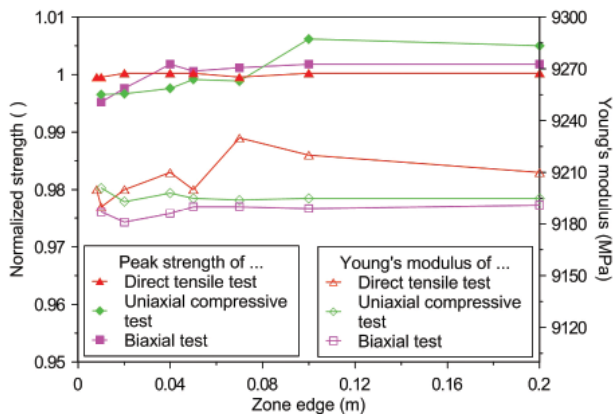


Figure 9. Effect of zone edge length on normalized peak strength for the continuum model.

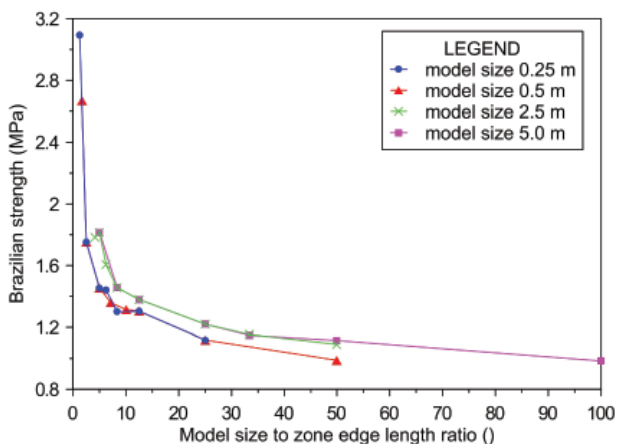


Figure 10. Dependence between Brazilian strength and model sample size to zone edge length ratio for four model sizes (diameter) for the continuum model.

As shown in Fig. 10, stabilization of the Brazilian strength occurs in the range of model size to zone edge length ratio between 25 and 35 (with a scatter error in the range of 5 %). Higher ratios lead to a longer calculation time, with only small improvements in the model prediction. The reason for the decreasing trend of the Brazilian strength was already discussed in Section 4.1.

On the other hand, the mesh density slightly influences the material behaviour in the Voronoi model, as shown in Fig. 11. The normalized strength is dependent on the ratio between the Voronoi edge length and the zone edge length. Since the zone edge length is defined as the maximum edge length of the triangular zones, there will be a critical limit with regard to the Voronoi edge length (i.e., the zone edge length is smaller, or equal, to the Voronoi edge length). When the ratio is less than one, there is no influence on the peak strength, regardless of the increasing value of the zone edge length, because the zone edge length is now limited by the Voronoi edge length.

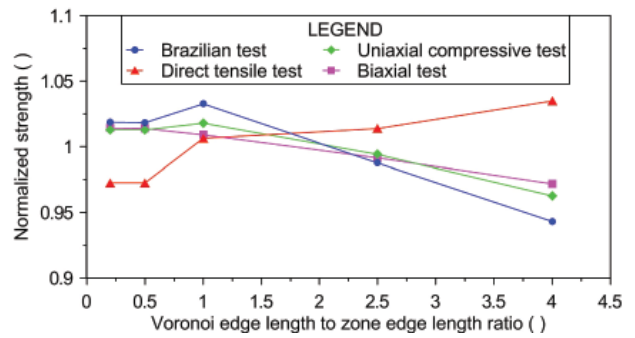


Figure 11. Effect of Voronoi edge length to zone edge length ratio on normalized peak strength for the Voronoi model.

With the ratio increasing from 1 to 4, the peak strength decreases by about 5 % for all the tests, except for the direct tensile test, where it increases by the same amount. A possible reason for this could be that the direct tensile test has a tensile stress state that is in contrast to the other three tests, where we have predominantly compressive stress states. Also, the peak strength scatter between the different seed numbers at an arbitrary mesh density is approximately 5 % of RSD. Based on these findings and to avoid long calculation times, the appropriate ratio of the Voronoi edge length to the zone edge length is between 1.5 and 4.

4.4 Number of fixed grid points

As discussed in Section 3.1, the velocity is applied to grid points (called fixed grid points) on the top side of the sample. In the rectangular-shaped model samples the number of fixed grid points is related to the mesh density in the continuum model and to both the mesh density and the polygon size in the Voronoi model. Therefore, the number of fixed grid points is a consequence of the mesh and polygon density and has no direct influence on the model's behaviour.

On the other hand, the circular geometry of the Brazilian test model contains several edges along the outer boundary. Besides the mesh density and polygon size, the number of edge segments is related to the number of fixed grid points in the upper and lower external boundaries. Increasing the number of segments implies an increase in the number of fixed grid points in both models. The results of the sensitivity analysis show that an increase in the number of fixed grid points will increase the Brazilian strength until stabilization is reached (Fig. 12 on next page). An up to 10 % RSD error can be expected in the stable region. Therefore, at least 4 fixed grid points (Fig. 12b) or 80 segments (Fig. 12a) are recommended values for both the continuum and Voronoi models.

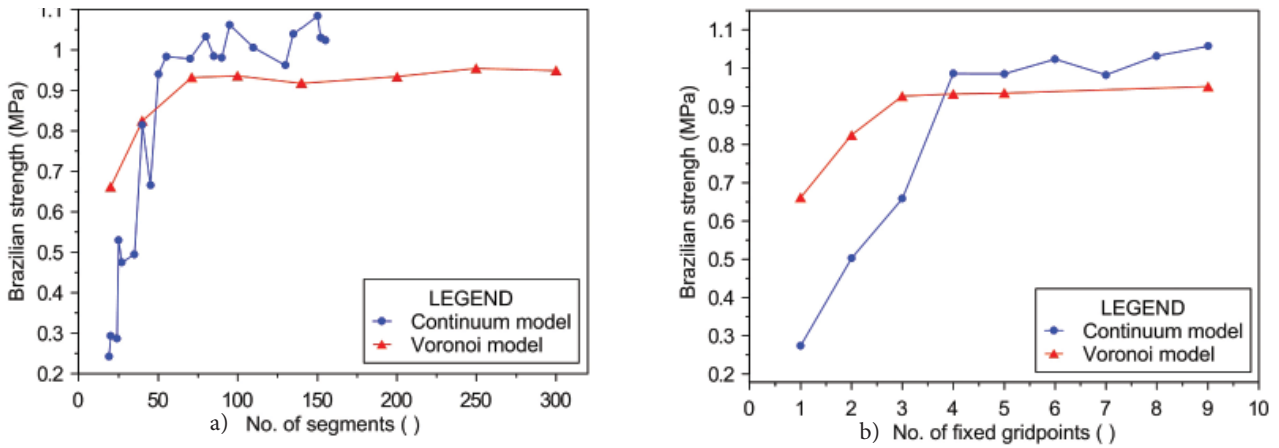


Figure 12. Effect of (a) number of segments and (b) number of fixed grid points on the Brazilian strength for the Voronoi model.

4.5 Strain rate

In accordance with the ISRM [33], a quasi-static laboratory compression test is achieved within the strain-rate interval 10^{-5} to 10^{-4} /s. Faster or slower strain rates than these can have a significant impact on the material's behaviour [34]. A similar response is observed in numerical simulations. Running a model test with a high applied velocity introduces dynamic effects in the simulation. However, choosing a very low strain rate is inefficient and leads to very time-consuming calculations. The aim of this part of the sensitivity analysis is to find the optimal strain rate for the current modelling study.

The optimal applied velocity can be determined using a trial-and-error procedure based on a comparison between the different stress-strain curves obtained from tests running at different velocities. As the maximum

applied velocity for which the shape of the stress-strain curve stabilizes and the peak strength becomes constant, the applied velocity can be adopted as the optimal velocity for the current model analysis. However, dealing with velocity is not very convenient when trying to compare the results between the different model tests. In that case it is better to use the displacement rate $\Delta \epsilon_r$, which can be calculated based on the number of cycles N_{cyc} needed for the current model analysis at the chosen applied velocity $\Delta \dot{u}_r$ and the mechanical time step Δt_m taken by UDEC:

$$\Delta \epsilon_r = \Delta \dot{u}_r \cdot \Delta t_m / N_{cyc} \quad (8)$$

Several Voronoi model sizes with the same mesh density and model heterogeneity are tested. The results from the uniaxial compressive test simulations presented in Fig. 13a show that there is a relationship between the applied velocity in the Voronoi model and the size of the model.

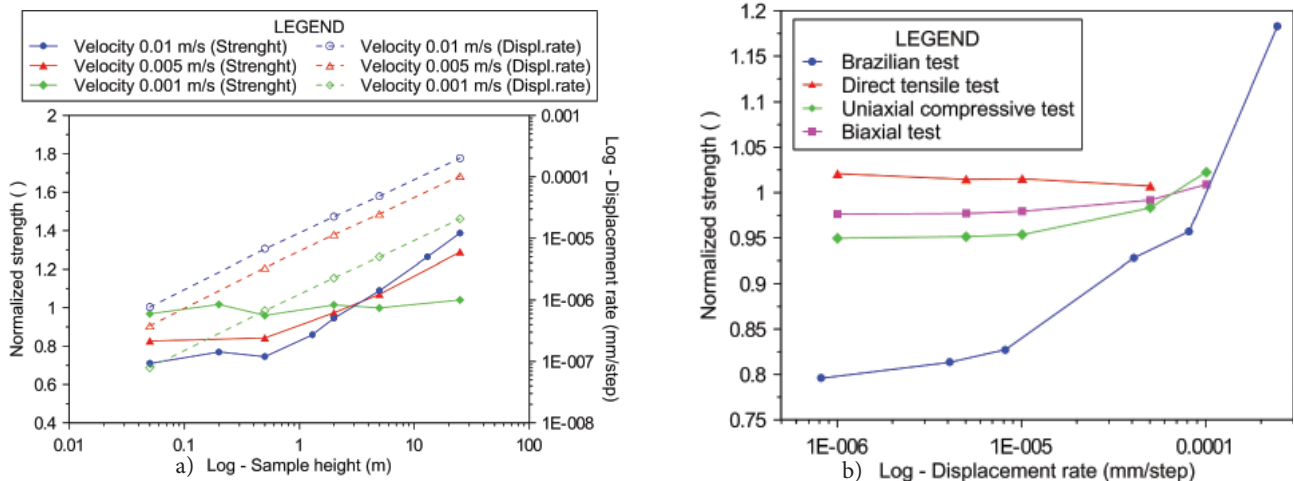


Figure 13. (a) Effect of applied velocity on normalized peak strength and displacement rate for different model sizes in uniaxial compressive test in the Voronoi model, and (b) effect of applied velocities on normalized peak strength in the continuum model.

Larger model sizes require a lower applied velocity than the smaller model sizes. That model behaviour is a result of the numerical algorithm of the distinct element code. Therefore, from that graph (Fig. 13a) an optimal displacement rate can be determined, regardless of the model size. For example, the peak strength stabilization of the solid blue line (an applied velocity of 0.01 m/s) is reached at a model size of approximately 0.5 m. Dragging a vertical line from here onto the dashed blue line shows that stabilization happens at approximately 10^{-5} mm/step, which can be adopted as an optimal displacement rate. A similar procedure can be used for an applied velocity of 0.005 m/s (red line). The peak strength of the tested sample with an applied velocity of 0.001 m/s is stable over the entire tested interval, because the displacement rate is lower than the optimal displacement rate.

To conclude, the optimal displacement rate should be 10^{-5} mm/step for all the model tests in this study. A similar displacement rate can be adopted for the continuum model (Fig. 13b) and for all the model tests performed in the numerical laboratory (Section 3).

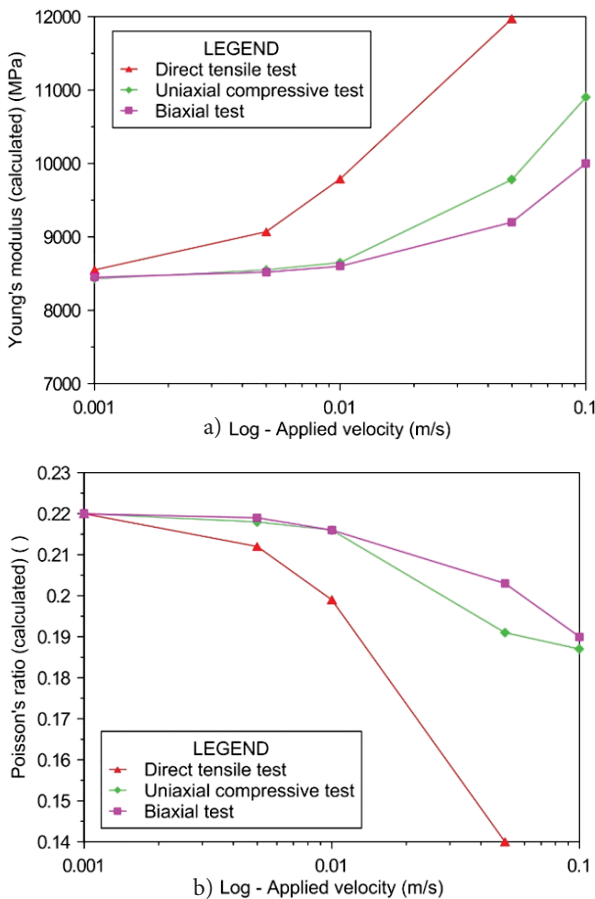


Figure 14. Effect of applied velocity on (a) Young's modulus and (b) Poisson's ratio for the Voronoi model.

The applied velocity also has a small influence on the Young's modulus and the Poisson's ratio. As can be seen in Fig. 14: at a high applied velocity the Young's modulus is higher, but the Poisson's ratio is lower. This can be interpreted as follows. At a high applied velocity (displacement rate) the model becomes stiffer (a higher Young's modulus), because it has less ability to accommodate all the deformation (a lower Poisson's ratio). On the other hand, at a low displacement rate, when the time step is small enough for the model to accommodate more of the deformation (higher Poisson's ratio), it becomes softer (lower Young's modulus). With a further decrease in the displacement rate the Young's modulus and the Poisson's ratio tend to stabilize.

4.6 Model shape aspect ratio

It is well documented that the sample shape influences the material strength and the ductility. As the aspect ratio of the height to width ($h:w$) increases, the strength and ductility decrease by decreasing the horizontal confinement stress in unconfined tests [35]. Due to the friction between the sample ends and the platen, and the difference between the elastic properties of the rock and the platen, the sample will be restrained near its ends and prevented from deforming uniformly [34].

Different rectangular-shaped model aspect ratios are tested under direct tensile, uniaxial compressive and biaxial test conditions. The results from the Voronoi model show that the peak strength decreases with an increasing aspect ratio (Fig. 15). In addition, the post-peak response becomes more ductile with a decreasing aspect ratio (Fig. 16). The peak strength stabilizes with an aspect ratio higher than 2, which is in accordance with the standard recommendations (i.e., a suggested

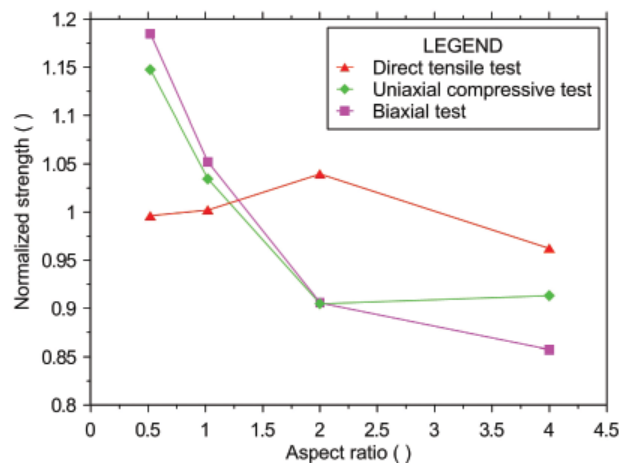


Figure 15. Effect of model shape aspect ratio ($h:w$) on the normalized peak strength for the Voronoi model.

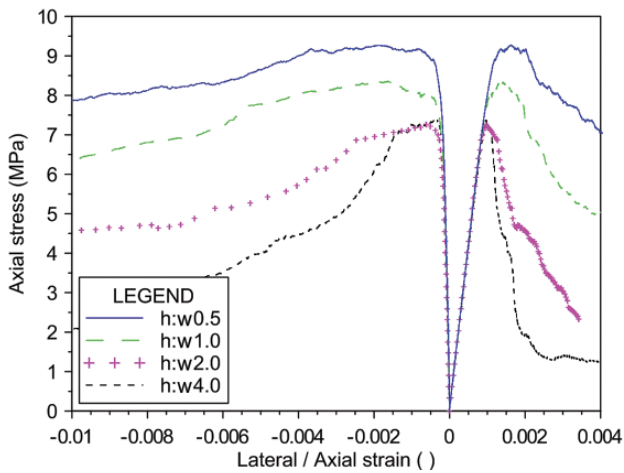


Figure 16. Uniaxial compressive test model stress-strain curves for different values of height to width ($h:w$) aspect ratio for the Voronoi model.

aspect ratio between 2.0 to 2.5 [36], and 2.5 to 3.0 [33]). As expected, the model aspect ratio has a negligible effect in direct tensile tests.

4.7 Material density

According to UDEC theory the internal density is irrelevant to the modelling in static systems since the internal forces in the system are low [23]. The material density only influences the calculation time, because it is proportionally related to the critical time step [23]. We have confirmed this for both the continuum and Voronoi models [28].

4.8 Deformability properties: Young's modulus, Poisson's ratio, normal and shear stiffness

The input Young's modulus and Poisson's ratio have a direct influence on the calculated Young's modulus and the Poisson's ratio in the continuum and Voronoi models. However, the input Young's modulus also influences the calculated Poisson's ratio in the Voronoi model as well. As can be seen in Fig. 17, an approximately 40 % change can be expected in the tested range. The explanation may be that a higher input Young's modulus causes the polygons to behave in a stiffer manner, so the majority of the deformation is accumulated by the contacts and thus the material's Poisson's ratio increases. When the input Young's modulus is lower, the polygons are softer and can accumulate the majority of the deformation, and thus the value of the calculated Poisson's ratio becomes lower. It is also shown that the Young's modulus has a negligible influence on the peak strength in all the model tests, except for the Voronoi model Brazilian test, where

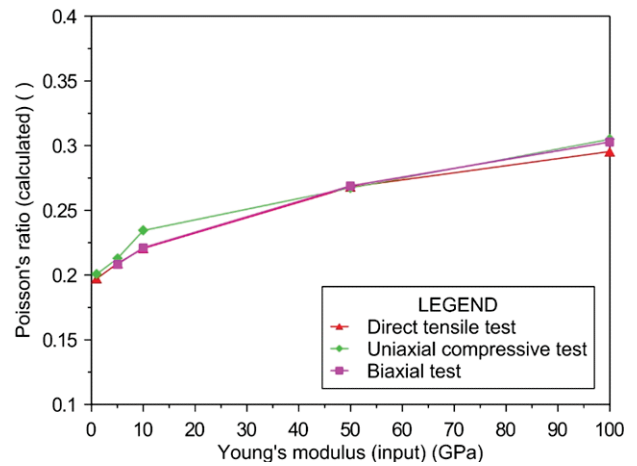


Figure 17. Effect of input Young's modulus on the calculated Poisson's ratio for the Voronoi model.

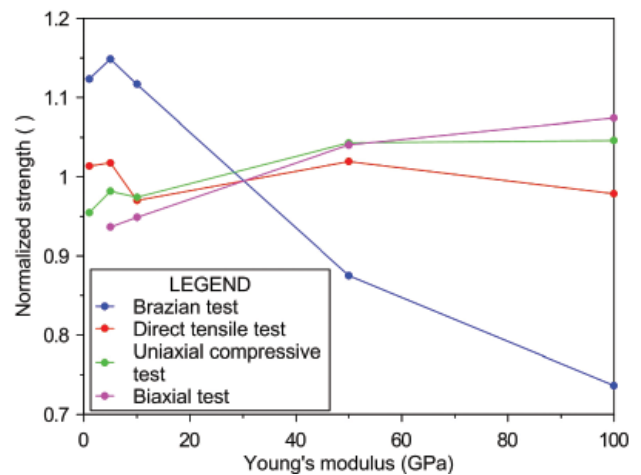


Figure 18. Effect of Young's modulus on normalized peak strength for the Voronoi model.

an increasing Young's modulus decreases the Brazilian strength by about 40 % in the tested range (Fig. 18).

In the Voronoi model the deformability is controlled by two additional micro-properties, i.e., the contact normal stiffness k_n and the contact shear stiffness k_s . However, both have an influence on the strength behaviour of the material as well. The effect of the normal and the shear stiffness are shown (Fig. 19) separately in terms of the normalised strength and stiffness ratios k_n/k_s and k_s/k_n . Different shapes of the peak-strength trend curves can be distinguished between the peak strengths measured in the tensile tests (e.g., the direct tension test and the Brazilian test) and the compressive tests (e.g., the uniaxial compressive test and the biaxial test). The compressive strength is slightly increasing throughout the tested interval, while the tensile strength quickly stabilizes. Observations of

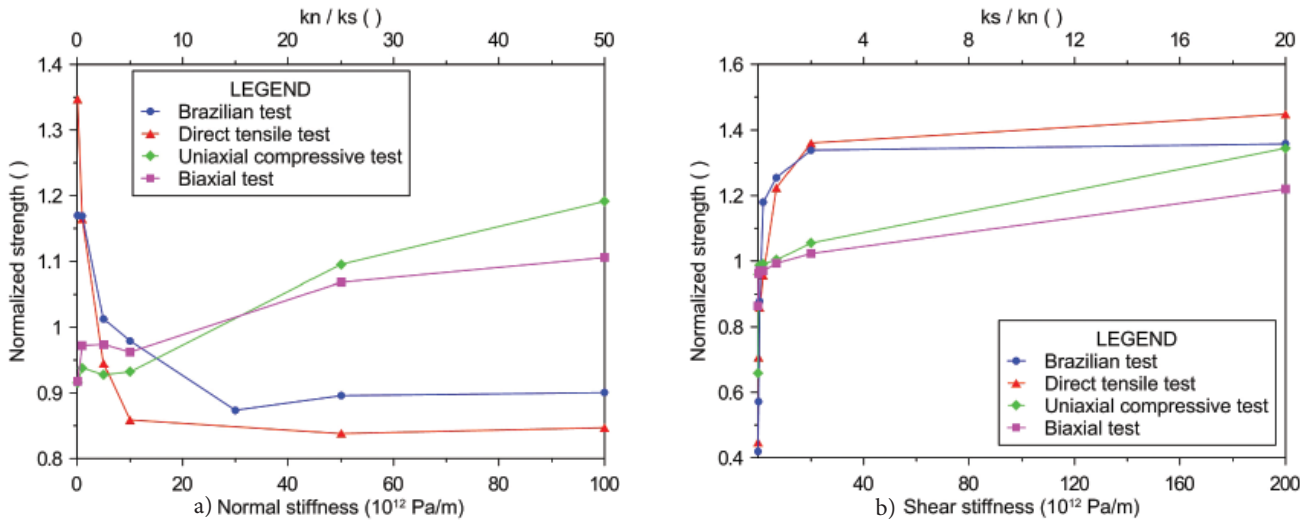


Figure 19. Correlation between normalized peak strength to (a) normal stiffness and k_n/k_s ratio, and to (b) shear stiffness and k_s/k_n ratio for the Voronoi model.

the model’s material behaviour (e.g., the shape of the stress-strain curve) is in agreement with the intact rock behaviour known from the laboratory if the stiffness ratio k_n/k_s is approximately between 1 to 20 (i.e., the stiffness ratio k_s/k_n is approximately between 1.0 and 0.05).

The empirical equation developed by D. Martin and reported by Vallejos et al. [14] and the data reported by Li & Wong [37] show that the laboratory-measured Brazilian strength is consistently higher than the direct tensile strength [28], most likely due to the friction between the platen and the sample ends, which causes confinement stress in the sample. The aim of our study is not to quantify the strength ratio, but only to check the trends observed in the laboratory, i.e., whether the simulated Brazilian strength is lower, higher or the same compared to the direct tensile strength. It is found that

the laboratory-measured strength ratios between the Brazilian tests and the direct tensile tests can be matched by choosing an appropriate stiffness ratio k_n/k_s . It is difficult to define a reasonable interval, because it is dependent on other input micro-properties as well, but is in between $k_n/k_s = 1$ to 20 range. In fact, the tensile-to-compressive strength ratio is also influenced by the stiffness ratio k_n/k_s and by other micro-properties (e.g., cohesion, friction angle, and tensile strength limit).

The normal to shear stiffness ratio can control the Young’s modulus and the Poisson’s ratio, as has been already recognized by Kazerani & Zhao [24] and in the BPM model [10, 17]. When the stiffness ratio is higher than a critical value, the calculated elastic properties become constant, even if the normal and/or the shear stiffness changes (Fig. 20, Fig. 21). Therefore, the stiff-

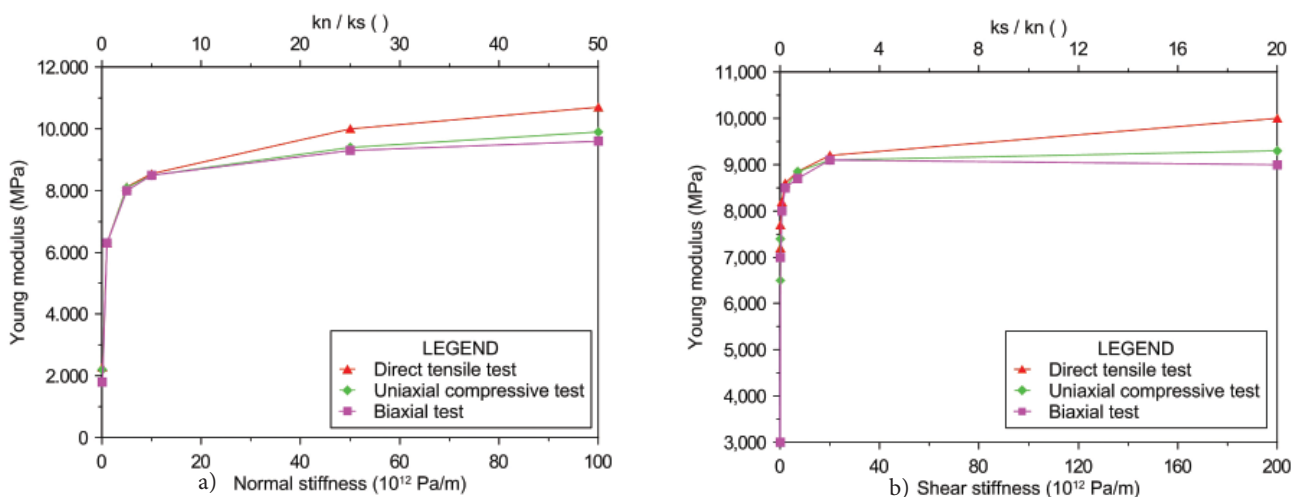


Figure 20. Correlation between Young’s modulus to (a) normal stiffness and k_n/k_s ratio, and to (b) shear stiffness and k_s/k_n ratio for the Voronoi model.

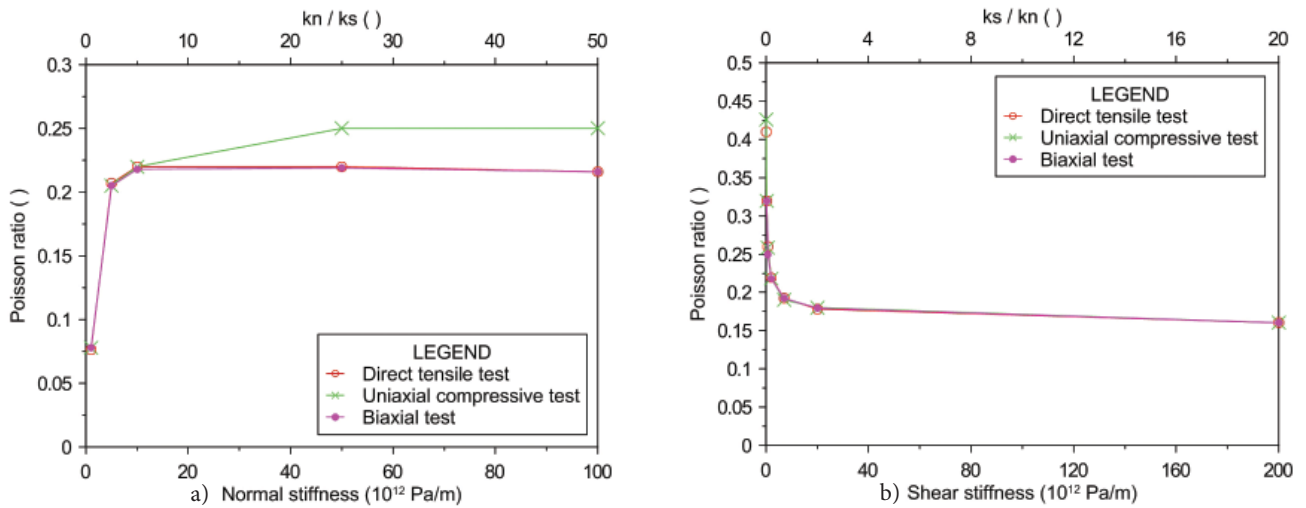


Figure 21. Correlation between Poisson's ratio to (a) normal stiffness and k_n/k_s ratio, and to (b) shear stiffness and k_s/k_n ratio for the Voronoi model.

ness ratio can be calibrated to some extent to fit the material's Poisson's ratio and the Young's modulus.

4.9 Strength properties: cohesion, friction angle and tensile strength limit

In Voronoi models, micro-properties, such as the contact cohesion, contact friction angle and contact tensile strength limit of the Voronoi polygonal contacts, exert the main control over the material's strength behaviour. In the continuum model the material's strength behaviour is controlled by the (macro) cohesion, the (macro) friction angle and the (macro) tensile strength limit. This is confirmed by the series of sensitivity analyses presented in this section.

First, the sensitivity analysis on cohesion is discussed. As shown in Fig. 22 a similar model response can be observed in both the continuum and the Voronoi models. The uniaxial or biaxial compressive strength show a linear dependence on increasing cohesion, which is controlled by the shear yield function. However, the Brazilian and direct tensile strength are controlled either by the tension or the shear yield function, as shown in Fig. 23. At first, when the cohesion is lower than the tensile strength limit (which can be an unrealistic case), it shows a linear dependence on the tensile strength and is controlled by the shear yield function (Fig. 23a). Once the tensile strength limit is reached (which is a more realistic case), the calculated peak tensile strength becomes constant, regardless of the cohesion increase and is controlled by the tension yield function (Fig. 23c).

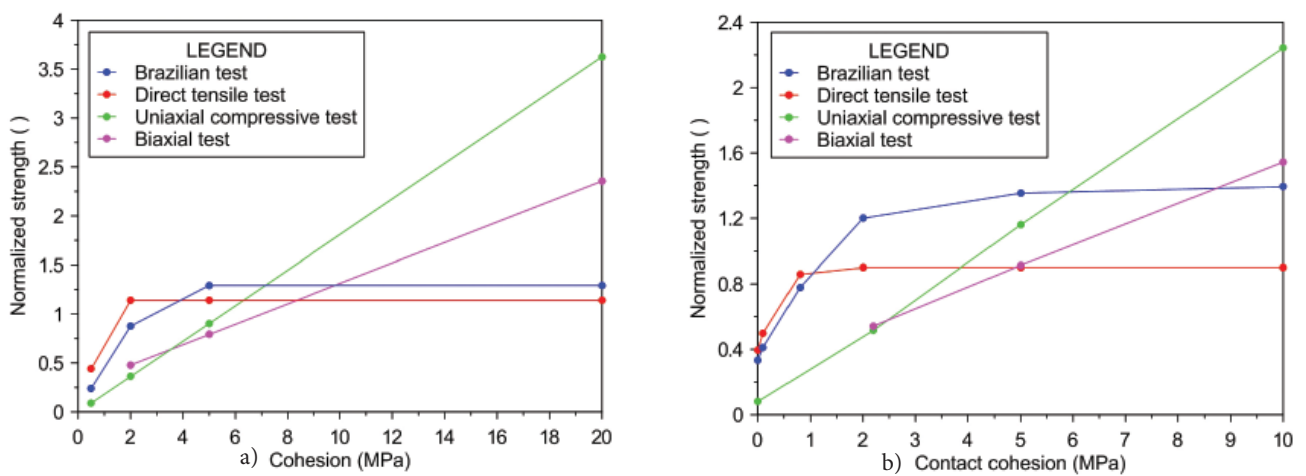


Figure 22. Correlation between cohesion and normalized peak strength for (a) the continuum and (b) the Voronoi model.

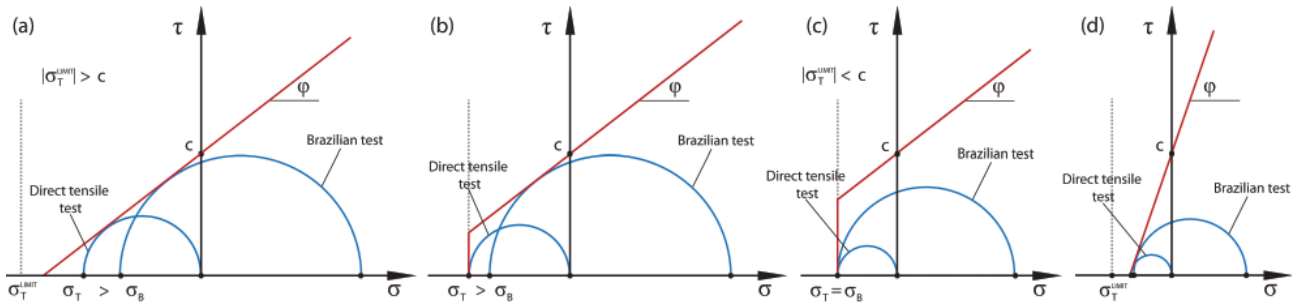


Figure 23. Schematic presentation of Mohr circles at (a) (absolute) high tensile strength limit, (b) similar values of cohesion and tensile strength limit, (c) high cohesion and (d) high friction angle.

Moreover, a relatively high cohesion compared to the tensile strength limit could produce undesirable post-peak behaviour in terms of a strong material resistance during sliding, which generates residual stresses that are commonly higher than the peak strength (mostly in the Brazilian test model). In this sense, the material model's behaviour is in agreement with the intact rock behaviour known from the laboratory if the cohesion values are approximately up to five times the tensile strength limit.

Similar to the sensitivity analysis of cohesion, the continuum and the Voronoi model show comparable results with respect to the friction angle (Fig. 24). The uniaxial and biaxial compressive strength show an exponential dependence on the increasing friction angle, which is controlled by the shear yield function. The Brazilian and direct tensile strength, on the other hand, is controlled either by the tension or the shear yield function. At low and moderate friction angles the direct tensile strength is constant and is controlled by the tensile yield function (Fig. 23c). However, a small decrease in the Brazilian strength is observed at low friction angles, which is more obvious in the continuum model (Fig. 24a). At present,

such a response is not fully understood. On the other hand, very high friction angles (which may not be a realistic case) induce a decrease in the tensile strength as well, but this time the shear yield function controls the response (Fig. 23d).

The sensitivity analysis has also shown that high friction angles can induce a strong shear resistance in the post peak, so that the residual shear strength exceeds the peak shear strength (Fig. 25). If such a post-peak behaviour is undesirable, it can be limited by choosing lower friction angles as the input (micro) property.

The major difference between both models is seen in the parametric sensitivity analysis of the tensile strength limit. The continuum model shows a very similar response to that of the sensitivity analysis of cohesion, except that the (uniaxial or biaxial) compressive strength is unaffected by the tensile strength limit (Fig. 26a). The Brazilian strength and the direct tensile strength exhibit a clear dependence upon the tensile strength limit (Fig. 26a). At first, when the tensile strength limit is low, the (macro) tensile strength is

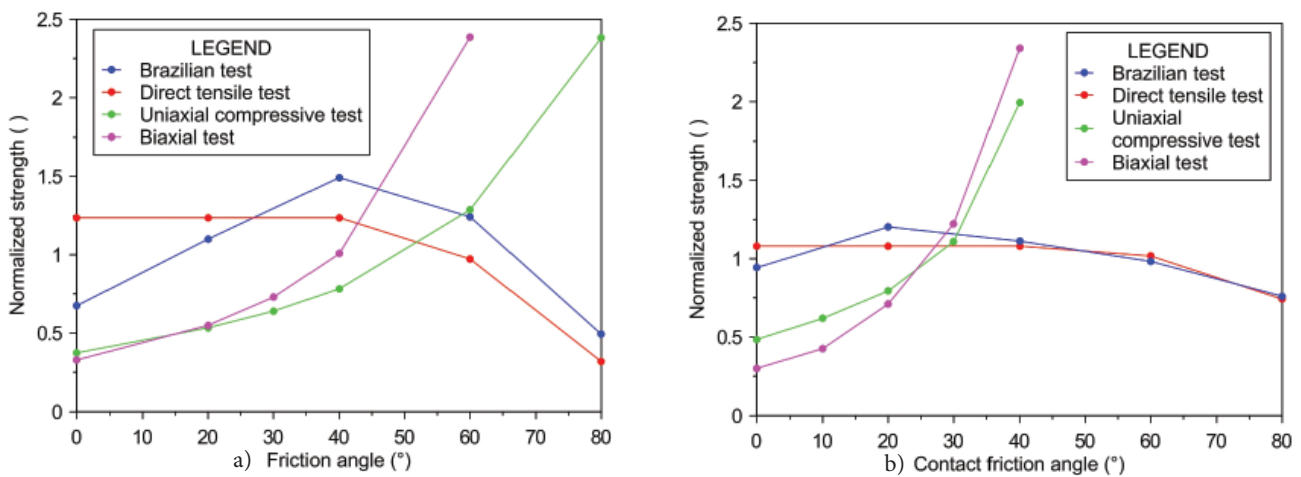


Figure 24. Correlation between friction angle and normalized peak strength for (a) the continuum and (b) the Voronoi model.

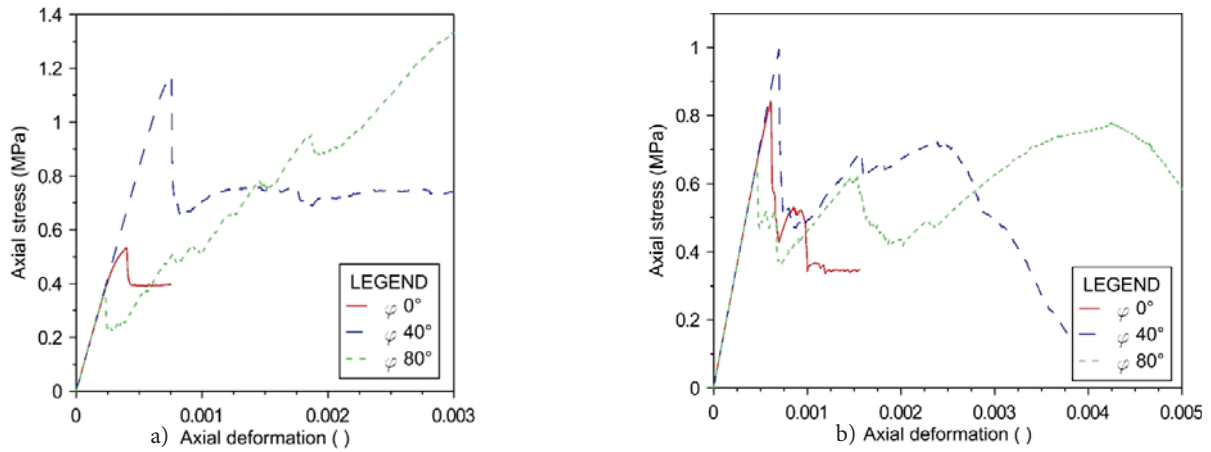


Figure 25. Effect of friction angle on stress-strain curves of Brazilian test model for (a) the continuum and (b) the Voronoi model.

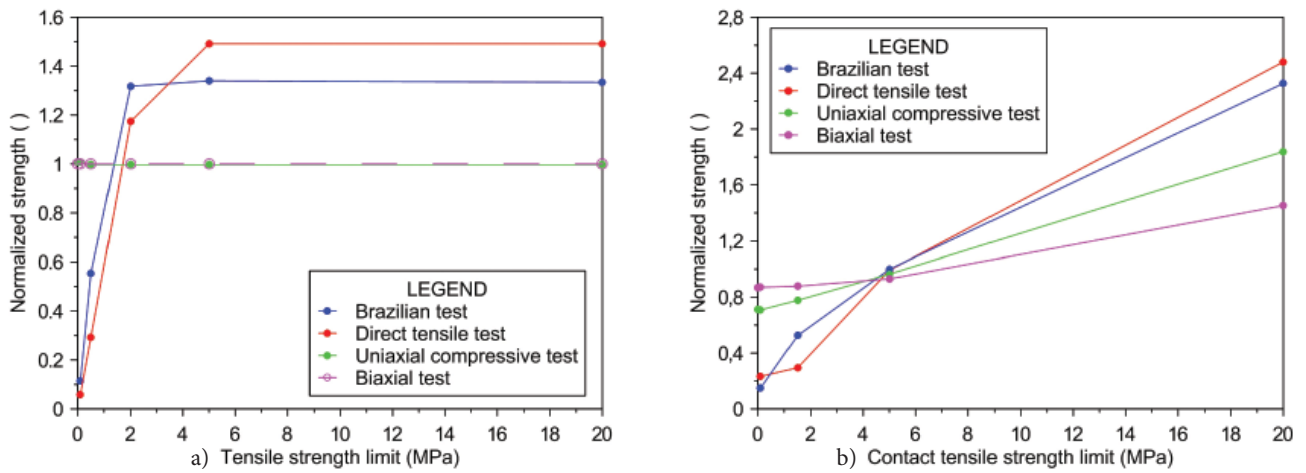


Figure 26. Correlation between tensile strength limit and normalized peak strength for (a) the continuum and (b) the Voronoi model.

controlled by the tension yield function (Fig. 23c). After reaching the critical value, e.g., the maximum tensile strength ($\sigma_t^{max} = c/\tan\phi$), the tensile strength becomes constant and the failure is controlled by the shear yield function (Fig. 23a).

On the other hand, the Voronoi model shows a semi-linear dependence on the tensile strength limit (Fig. 26b). Increasing the magnitude of the tensile strength limit increases the failure strength in every model tested. At this point it is clear that the macro-strength behaviour of the Voronoi model is not directly controlled by the input value of each single micro-property (i.e., it needs to be calibrated as a whole because all the micro-properties interact in complex ways) unlike the continuum model. In fact, every micro-property has an influence on the model's response, and has to be taken into account during the material's calibration procedure.

Contrary to what is observed in the Voronoi model, the Brazilian strength can never overcome the direct tensile strength in the continuum model. The difference between the tensile strengths in the continuum model is mainly affected by the cohesion and the tensile strength limit. The direct tensile strength is higher than the Brazilian strength as long as the Mohr-Coulomb model does not include the tensile strength limit. This is satisfied when the tensile strength limit is much higher than the cohesion (which is basically an unrealistic case, see Fig. 23a) or when the cohesion and tensile strength limits are similar in magnitude (Fig. 23b). When the cohesion is significantly larger than the tensile strength limit (Fig. 23c), the Brazilian strength and the direct tensile strength are similar in magnitude. (It should be noted that the graphs in the paper do not show the absolute, but the normalized, strength values.) The Brazilian strength could slightly overcome the direct

tensile strength in some simulations due to the rough mesh density (Section 4.3) or an inappropriate number of circle segments (Section 4.4). The Brazilian strength to direct tensile strength ratio in the Voronoi model is described in Section 4.8.

4.10 Dilation

Since intact rock is represented as an assembly of polygons with micro strength properties at their contacts, the cracking and failure that occurs during loading can potentially reproduce macro dilation and control the material's macro strength.

For the Voronoi model, a sensitivity analysis on input dilation angle, which is assigned to contacts, shows no significant influence on the pre-peak region and the peak strength in both models (Fig. 27). After failure, when the polygons start to slide along their contacts, this causes the material to dilate so that a higher dilation angle produces a lower residual strength (Fig. 27b). As expected, dilation has no effect on direct tensile-test simulations [28], since polygons are only moving apart. On the contrary, in the continuum model, a higher dilation angle produces a higher residual strength (Fig. 27a). The reason is in the formulation of the Mohr-Coulomb constitutive model, where material with a larger dilation angle tends to follow a strain-hardening path.

5 CONCLUDING REMARKS

The numerical modelling of intact rock microstructures has received a lot of attention in the past two decades. It

has been recognized that rock microstructure is of key importance in intact rock behaviour. For this purpose a Voronoi polygonal-shaped model was used to generate the intact rock microstructure and simulate its response to four standard laboratory tests. A detailed parametric sensitivity analysis was performed to obtain an in-depth understanding of the model behaviour.

The findings from the parametric sensitivity analysis can be summarized as follows:

- The effect on the peak strength of the Voronoi polygon size resolution can be eliminated by having more than 10 polygons in the model sample's cross-section.
- Voronoi polygon heterogeneity and distribution can be controlled by the seed number and the number of iterations. Up to 250 iteration steps are necessary to produce a natural crack pattern, which is also different for different seed numbers.
- Voronoi polygons are discretized into deformable zones. The recommended ratio of Voronoi edge length to zone edge length is at least 1.5.
- The strain rate effect is affected by the model size and in this project it is eliminated when it is lower than 10^{-5} mm/step.
- The model shape height-to-width ratio affects the peak strength and the material ductility, which is in accordance with the laboratory experiments.
- The stiffness ratio k_n/k_s affects the rock peak strength, the Young's modulus and the Poisson's ratio. Reasonable material behaviour can be achieved if the stiffness ratio k_n/k_s is between 1 and 20. The stiffness ratio k_n/k_s control affects the Brazilian to direct tensile strength ratio as well.

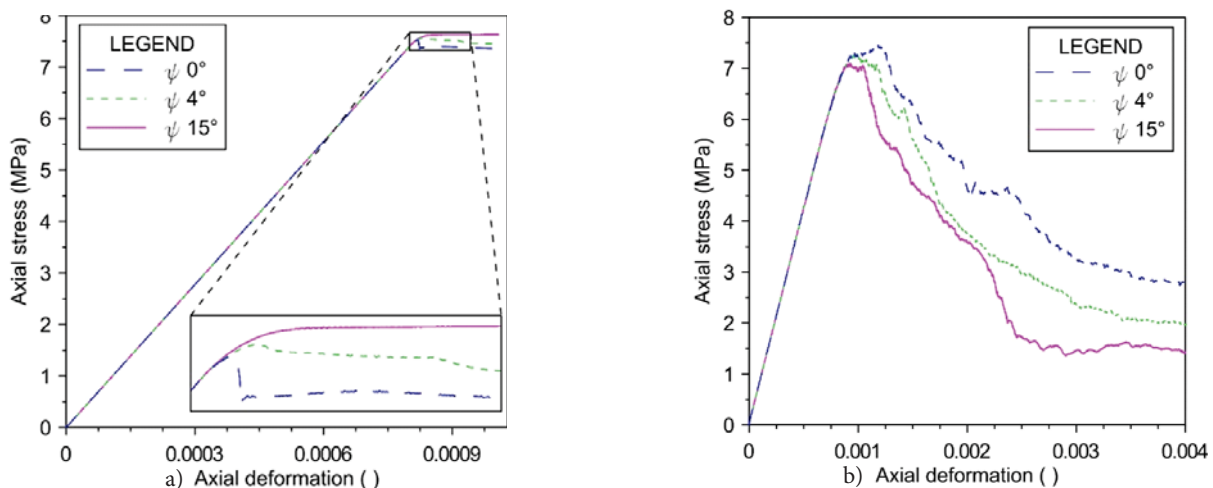


Figure 27. Effect of dilation on the stress-strain curves of the uniaxial compressive test for (a) the continuum and (b) the Voronoi model.

- Contact cohesion, contact friction angle and contact tensile strength limit affect the material's tensile and compressive peak strengths.
- Contact dilation affects the post-peak material behaviour.

In parallel with the Voronoi model, the continuum model was running as a benchmark, as it is widely known and used in many engineering applications. Since the Voronoi model can better represent the intact rock microstructure it was recognized that it could be a better approach to study damage processes in rocks during laboratory testing. Being able to control the model microstructure is one of its advantages. By using different seed numbers in the Voronoi models' generation, a slightly different crack pattern for the same conditions is reached. This makes it possible to match the model's macro response to real material behaviour not only quantitatively, but also qualitatively. This is not possible with the continuum model, because of its limitations as an elasto-plastic model and its linear failure envelope. Moreover, Voronoi models better reproduce the Brazilian to direct tensile strength ratio, and show a better representation of the dilation and post-peak behaviour in comparison to the continuum models.

Acknowledgements

The operation part of this research is financed by the European Union, European Social Fund. The authors also wish to thank the Itasca Education Partnership Program, Itasca International, Inc. and the Geotechnical Laboratory at the Institute for Mining, Geotechnology and Environment (IRGO, Slovenia). Mr. Abel Sánchez Juncal from Itasca Consultants AB is also greatly acknowledged for his contribution to various parts of this study.

REFERENCES

- [1] Marin, D. 1993. The strength of massive Lac du Bonnet granite around underground openings. PhD thesis. Canada: University of Manitoba.
- [2] Lan, H., Martin, C.D., Hu, B. 2010. Effect of heterogeneity of brittle rock on micromechanical extensile behavior during compression loading. *J. Geophys. Res.* 115(B1):B01202.
- [3] Mahabadi, O.K., Randall, N.X., Zong, Z., Grasselli, G. 2012. A novel approach for micro-scale characterization and modeling of geomaterials incorporating actual material heterogeneity. *Geophys. Res. Lett.* 39, L01303.
- [4] Van de Steen, B., Vervoort, A., Napier, J.A.L., Durrheim, R.J. 2003. Implementation of a flaw model to the fracturing around a vertical shaft. *Rock Mech. Rock Eng.* 36, 143–161.
- [5] Chen, S., Yue, Z.Q., Tham, L.G. 2007. Digital image based approach for three-dimensional mechanical analysis of heterogeneous rocks. *Rock Mech. Rock Eng.* 40, 145–168.
- [6] Potyondy, D.O. 2010. A Grain-Based Model for Rock: Approaching the True Microstructure. *Proceedings of Rock Mechanics in the Nordic Countries, Kongsberg, Norway*, pp. 10.
- [7] Tang, C.A. 1997. Numerical simulation on progressive failure leading to collapse and associated seismicity. *Int. J. Rock Mech. Min. Sci.* 34(2), 249–261.
- [8] Lui, H. 2003. Numerical Modelling of the Rock Fracture Process under Mechanical Loading. PhD thesis. Sweden: Luleå University of Technology.
- [9] Wang, S.Y., Sloan, S.W., Huang, M.L., Tang, C.A. 2011. Numerical Study of Failure Mechanism of Serial and Parallel Rock Pillars. *Rock Mech. Rock Eng.* 44, 179–198.
- [10] Potyondy, D.O., Cundall, P.A. 2004. A bonded-particle model for rock. *Int. J. Rock Mech. Min. Sci.* 41, 1329–1364.
- [11] Itasca Consulting Group, Inc. 2008. PFC 3D, Particle Flow Code in 3 Dimensions. 4th ed. Minneapolis, USA.
- [12] Kazerani, T., Zhao, J. 2013. A Microstructure-Based Model to Characterize micromechanical Parameters Controlling Compressive and Tensile Failure in Crystallized Rock. *Rock Mech. Rock Eng.* 47(2), 435-452.
- [13] Kazerani, T. 2013. A discontinuum-based model to simulate compressive and tensile failure in sedimentary rock. *J. Rock Mech. Geotech. Eng.* 5, 378-388.
- [14] Vallejos, J.A., Brzovic, A., Lopez, C., Bouzeran, L., Mas Ivars, D. 2013. Application of the Synthetic Rock Mass approach to characterize rock mass behavior at the El Teniente Mine, Chile. *Continuum and Distinct Element Numerical Modeling in Geomechanics. Minneapolis, Paper 07-02.* pp.15.
- [15] Brzovic, A., Schachter, P., de los Santos, C., Vallejos, J., Mas Ivars, D. 2014. Characterization and Synthetic Simulations to Determine Rock Mass Behaviour at the El Teniente Mine, Chile. Part I. *Proceedings, Caving 2014, 3rd International Symposium on Block and Sublevel Caving, Santiago, Chile*, pp. 8.
- [16] Vallejos, J., Suzuki, K., Brzovic, A., Mas Ivars, D. 2014. Characterization and synthetic simulations to determine rock mass behaviour at the El Teniente mine, Chile. Part II. *Proceedings, Caving*

- 2014, 3rd International Symposium on Block and Sublevel Caving, Santiago, Chile, pp. 9.
- [17] Diederichs, M.S. 1999. Instability of hard rock masses: the role of tensile damage and relaxation. PhD thesis. Canada: University of Waterloo.
- [18] Cho, N., Martin, C.D., Sego, D.C. 2007. A clumped particle model for rock. *Int. J. Rock Mech. Min. Sci.* 44, 997–1010.
- [19] Sheorey, P.R. 1997. Empirical rock failure criteria. Rotterdam: Balkema.
- [20] Vutukuri, V.S., Lama, R.D., Saluja, S.S. 1974. Handbook on mechanical properties of rocks, testing techniques and results, Vol I. Trans Tech Publications.
- [21] Bahrani, N., Potyondy, D., Pierce, M. 2012. Simulation of Brazilian Test Using PFC2D Grain-Based Model. Proceedings of 21st Canadian Rock Mechanics Symposium (CARMA), Quebec, Canada, pp. 485-493.
- [22] Potyondy, D.O. 2012. A flat-jointed bonded-particle material for hard rock. In: Proceedings of 46th U.S. Rock Mechanics/Geomechanics Symposium, Chicago, USA, pp. 10.
- [23] Itasca Consulting Group, Inc. 2014. UDEC, Universal Distinct Element Code. 4th ed. Minneapolis, USA.
- [24] Kazerani, T., Zhao, J. 2010. Micromechanical parameters in bonded particle method for modeling of brittle material failure. *Int. J. Numer. Anal. Meth. Geomech.* 34, 1877–1895.
- [25] Alzo'ubi, A.K. 2012. Modeling of rocks under direct shear loading by using discrete element method. *AHU. J. of Engineering & Applied Sciences*, 4(2), 5-20.
- [26] Gao, F. 2013. Simulation of Failure Mechanisms around Underground Coal Mine Openings Using Discrete Element Modelling. PhD thesis. Canada: Simon Fraser University.
- [27] Labuz, J.F., Zang, A. 2012. Mohr–Coulomb Failure Criterion. *Rock Mech. Rock Eng.* 45, 975–979.
- [28] Fabjan, T. 2015. Numerical modelling of mechanical properties of discontinuities in jointed and heterogeneous rock mass. PhD thesis. Slovenia: University of Ljubljana.
- [29] Bieniawski, T.Z. 1977. Suggested Methods for Determining Tensile Strength of Rock materials. *Int. J. Rock Mech. Min. Sci. Geomech Abs.* 15(3), 99-103.
- [30] ASTM International 2013. Standard test method for compressive strength and elastic moduli of intact rock core specimens under varying states of stress and temperatures. ASTM D7012-13.
- [31] Fairhurst, C., Hudson, J. 1999. Draft ISRM suggested method for the complete stress-strain curve for intact rock in uniaxial compression. *Int. J. Rock Mech. Min. Sci.* 36(2), 279–289.
- [32] Yoshinaka, R., Osada, M., Park, H., Sasaki, T., Sasaki, K. 2008. Practical determination of mechanical design parameters of intact rock considering scale effect. *Eng. Geol.* 96, 173-186.
- [33] Bieniawski, T.Z., Franklin, J.A., Bernede, M.J., Duffaut, P., Rummel, F., Horibe, T., Broch, E., Rodrigues, E., Van Heerden, W.L., Vokler, U.W., Hansagi, I., Szlavin, J., Brady, B.T., Deere, D.U., Hawkes, I., Milanovic, D. 1979. Suggested methods for determining the uniaxial compressive strength and deformability of rock materials. *Int. J. Rock Mech. Min. Sci. Geomech. Abstr.* 16(2), 135–140.
- [34] Brady, B.H.G., Brown, E.T. 2006. *Rock Mechanics for underground mining*. 3rd ed. Dordrecht: Springer.
- [35] Hudson, J.A., Harrison, J.P. 2005. *Engineering rock mechanics an introduction to the principles*. Pergamon; Elsevier Science.
- [36] ASTM International. Standard Practice for Preparing Rock Core as Cylindrical Test Specimens and Verifying Conformance to Dimensional and Shape Tolerances. ASTM D 4543-08.
- [37] Li, D., Wong, L.N.Y. 2012. The Brazilian Disc Test for Rock Mechanics Applications: Review and New Insights. *Rock Mech. Rock Eng.* DOI 10.1007/s00603-012-0257-7.